Roles of GABA Signaling in Directing Basket Cell Axonal Projections Toward Purkinje Cells in the Cerebellum

Hideki Miwa (Hideki_Miwa@ncnp.go.jp)
Gunma University Graduate School of Medicine https://orcid.org/0000-0001-6015-3007
Ken Kobayashi
Hokkaido University School of Agriculture Graduate School of Agriculture Research Faculty of Agriculture: Hokkaido Daigaku Nogakubu Daigakuin Nogaku Kenkyuin Nogakuin
Shinobu Hirai
Tokyo Metropolitan Institute of Medical Science
Mitsuhiko Yamada
National Center of Neurology and Psychiatry
Masahiko Watanabe
Hokkaido University School of Medicine: Hokkaido Daigaku Daigakuin Igakuin
Haruo Okado
Tokyo Metropolitan Institute of Medical Science
Yuchio Yanagawa
Gunma University

Research

Keywords: cerebellum, development, GABA, GAD67, GAD65, basket cells

Posted Date: October 27th, 2020

DOI: https://doi.org/10.21203/rs.3.rs-95440/v1

Roles of GABA signaling in directing basket cell axonal projections toward Purkinje cells in the cerebellum

Running title: GAD67 deficiency in the cerebellum

Hideki Miwa*[,1,2,3], Ken Kobayashi[4], Shinobu Hirai[2], Mitsuhiko Yamada[1], Masahiko Watanabe[5], Haruo Okado[2], and Yuchio Yanagawa[3]

[1]Department of Neuropsychopharmacology, National Institute of Mental Health, National Center of Neurology and Psychiatry, Tokyo, Japan.
[2]Neural Development Project, Department of Brain Development and Neural Regeneration, Tokyo Metropolitan Institute of Medical Science, Tokyo, Japan.
[3]Department of Genetic and Behavioral Neuroscience, Gunma University Graduate School of Medicine, Maebashi, Japan.
[4]Research Faculty of Agriculture, Hokkaido University, Sapporo, Japan.
[5]Department of Anatomy, Hokkaido University School of Medicine, Sapporo, Japan.

*Correspondence to: Hideki Miwa, Molecular Neuropsychopharmacology Section, Department of Neuropsychopharmacology, National Institute of Mental Health, National Center of Neurology and Psychiatry, Tokyo 187-8553, Japan. E-mail: Hideki_Miwa@ncnp.go.jp.

Number of figures: 7

Number of tables: 0

Number of supplemental figures: 4

Number of supplemental tables: 0

Abstract

Gamma-aminobutyric acid (GABA) is a major inhibitory neurotransmitter in the central nervous system, synthesized by two isoforms of glutamate decarboxylase (GAD): GAD65 and GAD67. GABA may act as a trophic factor during brain development, but its contribution to the development and maturation of cerebellar neural circuits is not known. To understand the roles of GABA in cerebellar development and associated functions in motor coordination and balance, we examined GAD65 conventional knock out (KO) mice and mice in which GAD67 was eliminated in parvalbumin-expressing neurons (*PV-Cre*; *GAD67*$^{flox/flox}$ mice). We found aberrant subcellular localization of the Shaker-type K channel Kv1.1 in basket cell collaterals of *PV-Cre*; *GAD67* $^{flox/flox}$ mice and abnormal projections from basket cells to Purkinje cells in both mouse strains. Furthermore, *PV-Cre*; *GAD67* $^{flox/flox}$ mice exhibited abnormal motor coordination in the rotarod test. These results indicate that GABA signaling in the cerebellum during development is critical for establishing appropriate connections between basket cells and Purkinje cells and is associated with motor coordination in mice.

Keywords: cerebellum, development, GABA, GAD67, GAD65, basket cells

Introduction

The cerebellum is important for motor coordination and motor learning, emotion, and cognition [1]. Dysfunction of this brain region is associated with cerebellar ataxia [2] and neurodevelopmental diseases, including autism spectrum disorder [3]. The basic organization of neural circuits in the cerebellum and other regions in the central nervous system is established early during development [4,5], when they are particularly sensitive to genetic and environmental factors. However, the mechanisms underlying the relevant factors and their impacts remain incompletely understood.

Gamma-aminobutyric acid (GABA) is a major inhibitory neurotransmitter in the central nervous system that is also reportedly involved in neural tissue development, acting as a trophic factor [6]. GABA is synthesized by two isoforms of glutamate decarboxylase (GAD), GAD65 and GAD67 [7], which differ with respect to cofactor associations and subcellular localization. Once synthesized, GABA is packaged in synaptic vesicles by the vesicular GABA transporter (VGAT) for release into the synaptic cleft via exocytosis [8]. The role of GABA signaling in the development of neural circuits in the cerebellum has been examined in several GABA-related gene deletion and pharmacological mouse models [9–16]. However, GAD67 and VGAT knockout (KO) mice die during the perinatal period. Therefore, the specific roles of GAD67 and VGAT in cerebellar development and maturation remain unknown [9,11,12].

Here, we analyzed a GAD67 conditional KO mouse strain in which GAD67 was deleted in the subset of GABAergic neurons that express parvalbumin (PV), as well as a conventional GAD65 KO mouse strain, to investigate whether GABAergic

signaling contributes to the postnatal development and maturation of neural circuits in the cerebellum. We observed aberrant subcellular localization of the Shaker-type K channel Kv1.1 in basket cell collaterals and abnormal projections of basket cell collaterals toward Purkinje cells in both mouse strains. Furthermore, the mice with PV-specific GAD67 deletion displayed impaired motor coordination in the rotarod test. Our findings indicate that GABA signaling in the cerebellum during development is critical for the establishment of proper connections between basket cells and Purkinje cells, and for motor coordination in mice.

Materials and Methods

Animals

This study utilized four strains of genetically modified mice: *PV-Cre*; *VGAT*$^{flox/flox}$ mice, *PV-Cre*; *GAD67*$^{flox/flox}$ mice [17,18], GAD67 KO (*GAD67*$^{GFP/GFP}$) mice [19], and GAD65 KO mice [10]. *PV-Cre* BAC transgenic mice [20] were crossed with *VGAT*$^{flox/flox}$ mice [14] and *GAD67*$^{flox/flox}$ mice [21] to generate *PV-Cre*; *VGAT*$^{flox/flox}$ and *PV-Cre*; *GAD67*$^{flox/flox}$ mice, respectively. In behavioral tests, male *PV-Cre*; *GAD67*$^{flox/flox}$ mutant mice and male littermate controls (*GAD67*$^{flox/flox}$) were used. All experiments were performed in accordance with the guidelines of the National Center of Neurology and Psychiatry Animal Care and Use Committee and the Animal Care and Experimentation Committee of Gunma University. All efforts were made to minimize the number of animals used and their suffering.

Immunohistochemistry

The mice were deeply anesthetized with sodium pentobarbital (50 mg/kg body weight, intraperitoneal) and transcardially perfused with phosphate-buffered saline (PBS; pH 7.4) followed by 4% paraformaldehyde (PFA) in 0.1 M phosphate buffer (pH 7.4). The brains were removed, postfixed in the same fixative overnight at 4°C, and immersed in 15% and 30% sucrose in PBS overnight for cryoprotection. Free-floating sections (40 μm) were cut using a sliding microtome (REM-710; Yamato Kohki Industrial Co., Ltd., Japan) and incubated in PBS with 0.3% Triton X-100 and 1% bovine serum albumin (BSA) for 1 h at room temperature. Then, the sections were incubated for 12 h at room temperature with primary antibodies diluted in PBS with 0.3% Triton X-100, 2% BSA. The primary antibodies used were as follows: anti-parvalbumin antibody (1:1,000; Frontier Institute, Ishikari, Hokkaido, Japan), mouse anti-PV (1:4,000; Sigma, St. Louis, MO, USA), monoclonal mouse anti-GAD67 (1:2,000; Millipore, Temecula, CA, USA), mouse anti-calbindin (1:1,000; Abcam, Cambridge, MA, USA), rabbit anti-vesicular glutamate transporter 1 (VGluT1) (1:4,000; Frontier Institute), guinea pig anti-VGluT2 (1:4,000; Frontier Institute), rabbit anti-VGAT (1:1,000; Frontier Institute), monoclonal mouse anti-Kv1.1 (1:1,000; NeuroMab, Davis, CA, USA), monoclonal mouse anti-neurofilament (Nfl) (1:1,000, BioLegend, San Diego, CA, USA); rabbit anti-tyrosine hydroxylase (1:500; Millipore), guinea pig anti-aldolase (zebrin II) (1:4,000; Frontier Institute), and rabbit anti-GFAP (1:1,000, Sigma). The sections were washed in PBS and incubated for 2 h in a mixture of Alexa Fluor 488-, Alexa Fluor 555-, and Alexa Fluor 633-conjugaed species-specific secondary antibodies (Thermo Fisher Scientific, Waltham, MA, USA) diluted 1:500 in PBS with 0.3% Triton X-100 and 2% BSA. To visualize perineuronal nets, brain sections were incubated with the biotinylated lectin *Wisteria floribunda* agglutinin (WFA) (1:2,000; Vector Labs, Burlingame, CA, USA) at

4°C overnight. After washing in PBS, the sections were incubated with Alexa Fluor 488 conjugated to streptavidin for 20 min at room temperature. Antibodies against amino acid residues 139–172 of mouse GAD65 (NCBI Reference Sequence NP_032104) were produced in guinea pigs for the present study. Procedures for making these affinity-purified antibodies were reported previously [22].

For quantitative analysis, all images were captured with a confocal laser scanning microscope (FV1000; Olympus, Japan) using the same settings. The images were analyzed using ImageJ/Fiji software. For each cerebellar section, all PV-, calbindin-, and GAD67-positive cells in either the molecular layer or the Purkinje cell layer were visually identified, and the intensities of the immunoreactive signals from the cell somata in each section were measured. For VGluT1, the fluorescence intensities were measured within a square (100 × 100 μm) located in the middle of the molecular layer of the cerebellum. VGluT2-positive puncta within the same-size square were counted using the built-in Analyze Particles function in Fiji to calculate the number of VGluT2-positive puncta per 100 μm^2. VGAT-positive puncta were similarly counted within a 100 × 20 μm rectangle. The fluorescence intensities of Kv1.1 and Nfls were obtained from maximal intensity projections of stacks of 10 images using the built-in Plot Profile function in Fiji. Quantification of the fluorescence intensities was carried out without any adjustment of brightness/contrast.

Behavioral analyses

All behavioral tests were performed in male mutant and littermate control mice that were 12 weeks old at the start of testing. The mice were housed in a room with a 12 h

light/dark cycle (lights on at 7:00 a.m.) with access to food and water *ad libitum*. Behavioral testing was performed between 10:00 a.m. and 5:00 p.m. by investigators blinded to the genotypes. The body weights of the mice were taken before neurological screening from the least to most demanding test to minimize the influence of one test on subsequent tests as follows: wire hang tests, followed by footprint tests, and finally rotarod tests.

The wire hang test utilized a wire-mesh grid to assess balance. The mouse was placed on the wire mesh, which was then inverted with the mouse gripping the wire. The test was repeated and the latency to fall was recorded with a 60 s cutoff time; the data were averaged to obtain the final score.

For the footprint test, the hind feet of the mice were painted with acrylic paint, and the mice were allowed to walk along a 32 cm-long 10 cm-wide runway (with 10 cm-high walls). A fresh sheet of paper was placed on the floor of the runway for each run. Each mouse was tested twice. The footprint patterns of the hind paws were evaluated in terms of the following parameters: (i) stride length, which was measured as the average distance in forward movement between each stride; (ii) stance length, which was measured as the average distance between left and right hind footprints; and (iii) sway length, which was taken as the average perpendicular distance between each footprint.

For the rotarod test, a mouse was placed on a rod (3 cm diameter; O'Hara & Co., Ltd., Tokyo, Japan) and was tested under three conditions: (i) the rod was accelerated (4–40 rpm over 300 s; four trials per day at 2 h intervals for 2 consecutive days); (ii) the rod rotated at a low constant speed (5 rpm for 60 s; four trials per day at 2 h intervals); and (iii) the rod rotated at a high constant speed (10 rpm for 60 s; four trials

per day at 2 h intervals). The amount of time each mouse was able to maintain its balance on the rod was measured.

Statistics

Data are expressed as the means ± standard errors of the means (SEMs) and were analyzed by Welch's unpaired *t*-test and two-way repeated measures analysis of variance (ANOVA) unless otherwise stated. The log-rank test was also used. A *P*-value of <0.05 was accepted as statistically significant.

Results

Structure of the cerebellum in *PV-Cre*; *GAD67*$^{flox/flox}$ mice

We generated a conditional KO mouse line in which VGAT is deleted from neurons expressing PV, a calcium-binding protein expressed in major populations of cerebellar GABAergic neurons, including Purkinje cells, stellate cells, and basket cells [23,24]. These *PV-Cre*; *VGAT*$^{flox/flox}$ mice were used to investigate whether vesicular GABA release contributes to the postnatal development and maturation of neural circuits in the cerebellum. *PV-Cre*; *VGAT*$^{flox/flox}$ mice were viable but exhibited body weight loss until postnatal day 12 (P12), and then developed generalized convulsive seizures and died at around P14 ($n = 4$) (**Additional file 1**). Thus, we were not able to use these mice to study the role of GABA signaling in the maturation of the cerebellar circuits. Therefore, we used another mouse line in which GABA synthesis was disrupted in PV-expressing neurons by deletion of the gene encoding GAD67. The survival rate of homozygous *PV-Cre*; *GAD67*$^{flox/flox}$ mice was lower than that of the control *GAD67*$^{flox/flox}$ mice

because some *PV-Cre*; *GAD67*$^{flox/flox}$ mice developed epileptic seizures with a significantly higher risk of seizure-related sudden death. Approximately 20% of these mice died by 2 months of age [17,18]. Therefore, we used the *PV-Cre*; *GAD67*$^{flox/flox}$ mice that survived after such events in this study. There was no difference in mean body weights between surviving *PV-Cre*; *GAD67*$^{flox/flox}$ and *GAD67*$^{flox/flox}$ littermate controls (control, 21.6 ± 0.7 g, $n = 10$; *PV-Cre*; *GAD67*$^{flox/flox}$, 20.0 ± 0.6 g, $n = 9$; $P = 0.134$) (**Fig. 1a**). Next, we confirmed the Cre-mediated deletion of *GAD67* from PV-expressing neurons in the cerebellum by immunohistochemistry for GAD67, PV, and Cre (**Fig. 1b**). Cre recombinase was expressed in almost all PV-positive neurons (93.1% ± 2.0%, $n = 114$ PV-positive cells from three mice; **Fig. 1c**, left bar), and these neurons showed no GAD67 expression (**Fig. 1b**). All Cre-expressing cells were PV positive ($n = 106$ Cre-positive cells from three mice; **Fig. 1c**, right bar). The numbers of PV-positive cells were not different between *PV-Cre*; *GAD67*$^{flox/flox}$ and *GAD67*$^{flox/flox}$ littermate controls in the molecular layer ($P = 0.8462$) (**Fig. 1d**, left; control, 1,366 ± 100.7 cells/mm^2; *PV-Cre*; *GAD67*$^{flox/flox}$, 1332 ± 139.2 cells/mm^2; $P = 0.8462$) or in the Purkinje cell layer (**Fig. 1d**, right; control, 36.1 ± 2.1 cells/mm^2; *PV-Cre*; *GAD67*$^{flox/flox}$, 35.8 ± 1.8 cells/mm^2; $P = 0.9082$). Fluorescent staining for calbindin and DAPI in sagittal tissue sections revealed no gross abnormalities in cerebellar lobule patterning in *PV-Cre*; *GAD67*$^{flox/flox}$ mice (**Fig. 1e**). Further investigation of the architecture of the cerebellum revealed no difference in the molecular layer thickness (**Fig. 1f**; *GAD67*$^{flox/flox}$ controls, 141.4 ± 4.5 μm, $n = 10$ slices; *PV-Cre*; *GAD67*$^{flox/flox}$, 145.8 ± 6.5 μm, $n = 10$ slices; $P = 0.586$). These data indicate that GAD67-mediated GABA signaling in the cerebellum is not required for proper layering of the cerebellar cortex.

We next performed immunohistochemistry of GAD67, GAD65, and calbindin (CB) (**Fig. 2a**). The specificity of the signals obtained with the anti-GAD67 and anti-GAD65 antibodies was confirmed using sections from *GAD67* KO mice and *GAD65* KO mice, respectively (**Additional file 2**). In the *PV-Cre*; *GAD67*$^{flox/flox}$ mice, no GAD67 signals were detected in the molecular layer (**Fig. 2b**, left; control, 39.7 ± 5.9 arbitrary units [a.u.], n = 8 slices from three mice; *PV-Cre*; *GAD67*$^{flox/flox}$, 5.2 ± 2.8 a.u., n = 8 slices from three mice; $P < 0.0001$); the Purkinje cell layer **(Fig. 2c**, left; control, 74.9 ± 14.0 a.u., n = 8 slices from three mice; *PV-Cre*; *GAD67*$^{flox/flox}$, 7.0 ± 2.9 a.u., n = 8 slices from three mice; $P < 0.0001$); or the deep cerebellar nuclei (**Fig. 2e**, left; control, 10.4 ± 0.9 a.u., n = 5 slices from two mice; *PV-Cre*; *GAD67*$^{flox/flox}$, 3.3 ± 0.3 a.u., n = 5 slices from two mice; $P < 0.0001$). However, GAD65 immunoreactivity in the molecular layer (**Fig. 2b**, right; control, 12.0 ± 0.7 a.u., n = 8 slices from three mice; *PV-Cre*; *GAD67*$^{flox/flox}$, 14.4 ± 2.6 a.u., n = 8 slices from three mice; $P = 0.3857$); the Purkinje cell layer (**Fig. 2c**, middle; control, 12.3 ± 0.5 a.u., n = 8 slices from three mice; *PV-Cre*; *GAD67*$^{flox/flox}$, 13.5 ± 2.2 a.u., n = 8 slices from three mice; $P = 0.6249$); and the deep cerebellar nuclei (**Fig. 2e**, middle; control, 27.7 ± 0.8 a.u., n = 5 slices from two mice; *PV-Cre*; *GAD67*$^{flox/flox}$, 29.6 ± 2.0 a.u., n = 5 slices from two mice; P = 0.4103) was not affected. Similarly, there were no significant differences in calbindin immunoreactivity in the Purkinje cell layer (**Fig. 2c**, right; control, 58.9 ± 8.1 a.u., n = 8 slices from three mice; *PV-Cre*; *GAD67*$^{flox/flox}$, 45.2 ± 6.6 a.u., n = 8 slices from three mice; $P = 0.2130$) or the deep cerebellar nuclei (**Fig. 2e**, right; control, 18.3 ± 0.4 a.u., n = 5 slices from two mice; *PV-Cre*; *GAD67*$^{flox/flox}$, 17.0 ± 0.8 a.u., n = 5 slices from two mice; $P = 0.1672$). Furthermore, we did not observe any differences in the perineuronal nets in the deep cerebellar nuclei [25] (**Additional file 3a**), tyrosine hydroxylase

234 expression within zebrin II-expressing zones [15] (**Additional file 3b**), or GFAP
235 expression in the cerebellar cortex (data not shown) compared with that in the control
236 *GAD67*$^{flox/flox}$ mice. Thus, deletion of *GAD67* from PV neurons successfully ablated
237 GAD67 expression in the cerebellum and did not induce compensatory expression
238 changes in GAD65 or calbindin.
239
240 **Normal VGluT1- and VGluT2-positive terminal densities**
241 GABAergic transmission regulates the formation and refinement of excitatory synaptic
242 inputs, including the elimination of climbing fiber synapses in the cerebellum during
243 development [13]. The two types of excitatory inputs onto Purkinje cells are
244 distinguished anatomically, as parallel fibers form synapses on secondary and tertiary
245 dendrites, whereas climbing fibers synapse on primary dendrites closer to the cell soma.
246 We performed immunohistochemistry to analyze parallel fiber and climbing fiber
247 terminals with anti-VGluT1 and anti-VGluT2 antibodies, respectively (**Fig. 3a**). There
248 was no significant difference in punctum immunoreactivity for VGluT1-positive
249 parallel fibers (**Fig. 3b**, top; control, 78.3 ± 18.6 a.u., n = 9 slices from three mice; *PV-*
250 *Cre*; *GAD67*$^{flox/flox}$, 95.0 ± 25.2 a.u., n = 9 slices from three mice; P = 0.1306) or the
251 number of VGluT2-positive climbing fiber terminals (**Fig. 3b**, bottom; control, 3.4 ± 0.2
252 per 100 μm^2, n = 9 slices from three mice; *PV-Cre*; *GAD67*$^{flox/flox}$, 2.9 ± 0.3 per 100
253 μm^2, n = 9 slices from three mice; P = 0.2378) between two genotypes, indicating that
254 GAD67-mediated GABA signaling in the cerebellum is not required for the
255 development of excitatory synaptic connections in the cerebellar cortex.
256
257 ***PV-Cre*; *GAD67*$^{flox/flox}$ mice develop abnormal basket cell projections**

We investigated whether GAD67 signaling affects the development and maturation of inhibitory terminals in the cerebellar cortex. The numbers of VGAT-immunoreactive puncta in the molecular layer of the cerebellar cortex did not differ between control *GAD67*$^{flox/flox}$ mice and *PV-Cre*; *GAD67*$^{flox/flox}$ mice (**Fig. 4**; control, 12.8 ± 1.9 per 100 μm^2, n = 8 slices from three mice; *PV-Cre*; *GAD67*$^{flox/flox}$, 12.7 ± 1.9 per 100 μm^2, n = 8 slices from three mice; P = 0.9775). We also examined the expression of Kv1.1 potassium channels, which are expressed in axons and terminals of cerebellar basket cells [26,27]. Specifically, we quantified the distribution of Kv1.1 immunoreactive signal intensities using line profiles up to 50 μm from the axon hillock (**Fig. 5a–c**). The results showed that the summated Kv1.1 signal intensity that was measured 10 μm from the axon hillock was higher in *PV-Cre*; *GAD67*$^{flox/flox}$ mice than in *GAD67*$^{flox/flox}$ controls (**Fig. 5d**; control, 1,711 ± 115.1 a.u., n = 6 slices from three mice; *PV-Cre;* *GAD67*$^{flox/flox}$, 2,243 ± 103.3 a.u., n = 6 slices from three mice; P = 0.0065). Furthermore, immunostaining for Nfl was performed to label basket cell collaterals [28] within 50 μm from the axon hillock (**Fig. 5e–g**). Similar to that for Kv1.1., the summated signal intensity for Nfl was higher for *PV-Cre*; *GAD67*$^{flox/flox}$ mice than for *GAD67*$^{flox/flox}$ controls (**Fig. 5h**; control, 7,607 ± 1,026 a.u., n = 8 slices from three mice; *PV-Cre*; *GAD67*$^{flox/flox}$, 11,276 ± 959 a.u., n = 8 slices from three mice; P = 0.0205). Taken together, these results suggest that the axonal projections from basket cells onto Purkinje cells are abnormal in *PV-Cre*; *GAD67*$^{flox/flox}$ mice

Abnormal cerebellar structure in *GAD65* KO mice

We also investigated the role of GAD65 in cerebellar development and maturation using *GAD65* KO mice (**Additional file 4**). As with *PV-Cre*; *GAD67*$^{flox/flox}$ mice, we did not detect any differences in PV-positive cell density or immunostaining for calbindin, VGluT1, VGluT2, or VGAT in the molecular layer of the cerebellum in *GAD65* KO mice. However, analyses of Kv1.1 distribution within 50 μm of the axon hillocks of Purkinje cells also revealed no difference between controls and *GAD65* KOs (**Fig. 6a–d**). Moreover, the summation of Kv1.1 signal intensity 10 μm from the axon hillock was comparable between the two genotypes (**Fig. 6d**; wild-type, 913.8 ± 157.2 a.u., n = 9 slices from three mice; *GAD65* KO, 960.4 ± 118.0 a.u., n = 9 slices from three mice; P = 0.8157). By contrast, the distributions of Nfl immunoreactive signal intensities within 50 μm from the axon hillock differed (**Fig. 6e–g**). The summated signal intensity for Nfl was higher for *GAD65* KO mice than for wild-type controls (**Fig. 6h**; wild-type, 4,709 ± 424 a.u., n = 9 slices from three mice; *GAD65* KO, 7,588 ± 846 a.u., n = 9 slices from three mice; P = 0.0105). Therefore, these results suggest that GAD65-mediated signaling also contributes to the projection of basket cell collaterals to Purkinje cells during development.

Impaired motor coordination in *PV-Cre*; *GAD67*$^{flox/flox}$ mice

To determine whether there were functional consequences of the abnormal cerebellar development in *PV-Cre*; *GAD67*$^{flox/flox}$ mice, we performed behavioral tests to assess motor function (**Fig. 7**). *PV-Cre*; *GAD67*$^{flox/flox}$ mice exhibited severe deficits in the accelerating rotarod test compared with the performance of the control mice [$F(1,17)$ = 57.07, $P < 0.0001$; **Fig. 7a**]. Although the mice performed similarly on a rod rotating at

303 a constant speed of 5 rpm [$F(1,17) = 3.29$, $P = 0.0875$; **Fig. 7b**], *PV-Cre*; *GAD67*$^{flox/flox}$
304 mice were quicker to fall than the control mice when the rod was rotating at 10 rpm
305 [$F(1,17) = 30.54$, $P < 0.0001$; **Fig. 7c**]. Analyses of their footprint patterns to examine
306 gait characteristics (**Fig. 7d**) revealed no differences between the genotypes with regard
307 to stride length (control, 5.2 ± 0.3 cm, $n = 10$; *PV-Cre*; *GAD67*$^{flox/flox}$, 5.0 ± 0.2 cm, $n =$
308 9; $P = 0.5073$), sway (control, 2.8 ± 0.1 cm, $n = 10$; *PV-Cre*; *GAD67*$^{flox/flox}$, 3.0 ± 0.1
309 cm, $n = 9$; $P = 0.2940$), and stance (control, 3.9 ± 0.2 cm, $n = 10$; *PV-Cre*;
310 *GAD67*$^{flox/flox}$, 3.8 ± 0.1 cm, $n = 9$; $P = 0.5162$) (**Fig. 7e**). In addition, muscular strength
311 was examined via a wire hang test, and no differences were observed between the
312 genotypes (control, 108.1 ± 18.1 s, $n = 10$; *PV-Cre*; *GAD67*$^{flox/flox}$, 77.1 ± 24.1 s, $n = 9$;
313 $P = 0.3191$; **Fig. 7f**). Whereas *PV-Cre*; *GAD67*$^{flox/flox}$ mice exhibit motor deficits,
314 *GAD65* KO mice show no motor deficits in the rotarod test [10], despite the observed
315 basket cell projection abnormalities. These results suggest that the motor deficit
316 exhibited by *PV-Cre*; *GAD67*$^{flox/flox}$ mice may be a result of the aberrant subcellular
317 localization of Kv1.1 at basket cell synapses on Purkinje cells as well as deficits in
318 GABA-mediated inhibitory synaptic inputs.
319

320 ## Discussion

321 The contribution of GAD-mediated GABA synthesis and GABA signaling to the
322 development and maturation of cerebellar neural circuits has been difficult to study
323 because of the lethality associated with the deficiency of GABAergic system-related
324 molecules in conventional genetic knockout mouse models [9, 11, 12]. Using the
325 Cre/loxP system, we conditionally knocked out *GAD67* from PV-expressing cerebellar

neurons and found that the distribution of the Shaker-type K^+ channel Kv1.1 was altered, resulting in the abnormal projection of basket cell collaterals onto Purkinje cells, a phenotype that was also observed in *GAD65* KO mice. GABA signaling is important for the development of the neural circuits in the cerebral cortex [29] and hippocampus [30,31]. To our knowledge, this is the first report describing the importance of GABA signaling for the development of inhibitory circuits in the cerebellum.

PV-Cre; *GAD67* knockout mice exhibited abnormal motor coordination in the rotarod test. These results suggest that GABA signaling in the cerebellum during development is critical for motor coordination and balance. Our findings support those of other studies on GABA signaling in the cerebellum. Mice heterozygous for *GAD67* (*GAD67*$^{+/GFP}$) [19] and mice with pharmacologically inhibited GAD activity show impaired climbing fiber elimination [13]. Mice with *VGAT* deficiency in Purkinje cells exhibit abnormal molecular zone structure and spinocerebellar afferent topography, and display motor dysfunctions in the rotarod test [14,15]. Mice with pancreas-specific transcription factor 1a (*Ptf1a*)-Cre-mediated deletion of *GAD67* show impaired inhibitory synaptic transmission but normal Purkinje cell morphology and synaptic densities in the cerebellar cortex [16]. However, the effect of these deletions on basket cell collaterals had not been investigated in detail. Nakayama et al. performed paired whole-cell recordings in *GAD67*$^{+/GFP}$ mice at P10–P12, revealing aberrant inhibitory inputs from basket cells to Purkinje cells [13]. However, adult *GAD67*$^{+/GFP}$ mice have normal motor coordination (our unpublished data); thus, it is not clear if these changes resolved in adulthood or there were compensatory mechanisms to mitigate motor deficits.

350 The present study shows that adult *PV-Cre*; *GAD67*$^{flox/flox}$ mice have aberrant
351 subcellular localization of Kv1.1, abnormal axonal projections from basket cells to
352 Purkinje cells, and impaired motor coordination. As *GAD65* KO mice also exhibited
353 abnormal basket cell projections, the results suggest that GAD-mediated GABA
354 synthesis and GABA signaling are important for the development of basket cell
355 collaterals. Although GABA has an inhibitory effect in adults, it has an excitatory effect
356 during the neonatal period because of the balance of chloride ion exchange [32]. We
357 show that deletion of *GAD67* from PV-expressing neurons as well as deletion of
358 *GAD65* alter basket cell projections to Purkinje cells, although it is not clear if this is
359 through inhibitory or excitatory actions. GAD67 is a constitutively active holoenzyme,
360 responsible for >90% of GABA synthesis [9,33]. By contrast, GAD65 is a
361 predominantly dormant apoenzyme that is activated rapidly upon the binding of
362 pyridoxal phosphate and thus is important for fast modulation of inhibitory synaptic
363 transmission during intense synaptic activity [34]. In addition, the expression of these
364 two GAD enzymes differs during postnatal development: GAD67 expression is
365 detectable at birth, whereas GAD65 is not expressed until P6 (as shown in the rat barrel
366 cortex) [35]. Basket cells begin to innervate the Purkinje cell layer after P7 [28,36].
367 These differences may explain the discrepancies between *PV-Cre*; *GAD67*$^{flox/flox}$ mice
368 and *GAD65* KO mice in terms of subcellular Kv1.1 distributions and behavioral
369 phenotypes.
370 Basket cell axons first contact the Purkinje cell soma and then move straight
371 to the axon initial segment without resting at the soma or climbing up the dendrites,
372 which involves ankyrin G, as this initial step is disrupted in ankyrin G KO mice [36].
373 Once the contacts are established, basket cells can modulate the firing rates of both

374 simple and complex spikes of Purkinje cells [37]. The results from the present study
375 indicate that GAD-mediated GABA signaling is also important for proper targeting of
376 basket cell projections to the Purkinje cells as well as proper localization of Kv1.1 at
377 presynaptic terminals during early development. In the cerebellar basket cells, K^+
378 channel α-subunits Kv1.1 and Kv1.2 are expressed in both axons and terminals
379 [26,27,38], and are co-assembled with cytoplasmic Kvβ2 subunits [39]. Trafficking and
380 cell surface expression of Kv1.2-containing Kv channels are regulated by
381 phosphorylation of Kv1.2 [40]. The GAD67 deficiency in *PV-Cre*; *GAD67*$^{flox/flox}$ mice
382 may result in depolarization-induced Kv1.2 phosphorylation and thus aberrant
383 subcellular localization of Kv1.1. However, further studies are needed to explore this as
384 well as to determine if the altered localization impacts the physiological functions of
385 basket cells.
386 Mutations in the gene encoding Kv1.1 (*KCNA1*) are responsible for episodic
387 ataxia type 1 [41–43]. We therefore attribute the abnormal motor coordination in *PV-*
388 *Cre*; *GAD67*$^{flox/flox}$ mice to the aberrant subcellular localization of Kv1.1 caused by
389 GAD67-mediated GABA signaling deficiency. Notable in this respect, autoantibodies to
390 GAD65 are associated with cerebellar ataxia [2,44]. Our results show that GAD65-
391 mediated GABA signaling alters the targeting of basket cell collaterals to Purkinje cells
392 without affecting the density of excitatory and inhibitory synaptic inputs in the
393 molecular layer or the density of PV-positive neurons. Thus, our findings and future
394 studies aimed at identifying the role of GABA signaling in basket cells will be useful
395 for further understanding the association between *KCNA1* mutations or anti-GAD
396 antibodies and cerebellar ataxia.

In conclusion, we show that the subcellular localization of Kv1.1 is altered in the cerebella of *PV-Cre*; *GAD67* knockout mice, and that the targeting of basket cell collaterals to Purkinje cells is disrupted in these mice as well as in *GAD65* KO mice. Furthermore, *PV-Cre*; *GAD67* knockout mice exhibited abnormal motor coordination in the rotarod test. Thus, our results indicate that GABA signaling in the cerebellum is critical for the development of cerebellar neural circuits in mice.

Declarations

Ethics approval

All animal experiments were performed in accordance with the guidelines of the National Center of Neurology and Psychiatry Animal Care and Use Committee and the Animal Care and Experimentation Committee of Gunma University.

Consent for publication

Not applicable.

Availability of data and materials

The materials used during the current study are available from the corresponding author upon reasonable request.

Competing interests

The authors declare that they have no competing interests.

Funding

This work was supported by Grants-in-Aid for Scientific Research from the Ministry of Education, Science, Sports, Culture and Technology of Japan, the Uehara Memorial Foundation, Nakatani Foundation, and Nakayama Foundation (to HM), and an Intramural Research Grant for Neurological and Psychiatric Disorders provided by the National Center of Neurology and Psychiatry, Japan (30-9) (to MY).

Author Contributions

HM and YY performed the research; KK, SH, MY, and HO contributed reagents/analytic tools; YY generated the *GAD67*-floxed and GAD65 KO mice; MW generated anti-GAD65 antibody, and HM analyzed the data and prepared the manuscript, which was approved by all authors.

Acknowledgments

We thank Dr. Nobuaki Tamamaki for kindly providing *PV-Cre* mice. We also thank Wataru Uno, Yu Kubota, Sota Hoshi, Reina Mizuma, the members of our laboratory, and the staff both at Division of Laboratory Animal Resources, National Center of Neurology and Psychiatry, and at the Institute of Experimental Animal Research, Gunma University Graduate School of Medicine, for technical assistance.

441 **References**

442 1. Ito M. Control of mental activities by internal models in the cerebellum. Nat Rev

443 Neurosci. 2008;9:304–13.

444 2. Manto M, Mitoma H, Hampe CS. Anti-GAD Antibodies and the Cerebellum: Where

445 Do We Stand? The Cerebellum. 2019;18:153–6.

446 3. Wang SSH, Kloth AD, Badura A. The Cerebellum, Sensitive Periods, and Autism.

447 Neuron. 2014;83:518–32.

448 4. Tau GZ, Peterson BS. Normal development of brain circuits.

449 Neuropsychopharmacology. 2010;35:147–68.

450 5. Hensch TK. Critical period plasticity in local cortical circuits. Nat Rev Neurosci.

451 2005;6:877–88.

452 6. Represa A, Ben-Ari Y. Trophic actions of GABA on neuronal development. Trends

453 Neurosci. 2005;28:278–83.

454 7. Soghomonian JJ, Martin DL. Two isoforms of glutamate decarboxylase: why?

455 Trends Pharmacol Sci. 1998;19:500–5.

8. Chen R, Wei J, Fowler SC, Wu JY. Demonstration of functional coupling between dopamine synthesis and its packaging into synaptic vesicles. J Biomed Sci. 2003;10:774–81.

9. Asada H, Kawamura Y, Maruyama K, Kume H, Ding R-G, Kanbara N, et al. Cleft palate and decreased brain γ-aminobutyric acid in mice lacking the 67-kDa isoform of glutamic acid decarboxylase. Proc Natl Acad Sci U S A. 1997;94:6496–9.

10. Asada H, Kawamura Y, Maruyama K, Kume H, Ding RG, Ji FY, et al. Mice lacking the 65 kDa isoform of glutamic acid decarboxylase (GAD65) maintain normal levels of GAD67 and GABA in their brains but are susceptible to seizures. Biochem Biophys Res Commun. 1996;229:891–5.

11. Wojcik SM, Katsurabayashi S, Guillemin I, Friauf E, Rosenmund C, Brose N, et al. A Shared Vesicular Carrier Allows Synaptic Corelease of GABA and Glycine. Neuron. 2006;50:575–87.

12. Saito K, Kakizaki T, Hayashi R, Nishimaru H, Furukawa T, Nakazato Y. The physiological roles of vesicular GABA transporter during embryonic development : a study using knockout mice. Mol Brain. 2010;3:40.

13. Nakayama H, Miyazaki T, Kitamura K, Hashimoto K, Yanagawa Y, Obata K, et al. GABAergic Inhibition Regulates Developmental Synapse Elimination in the Cerebellum. Neuron. 2012;74:384–96.

14. Kayakabe M, Kakizaki T, Kaneko R, Sasaki A, Nakazato Y, Shibasaki K, et al. Motor dysfunction in cerebellar purkinje cell-specific vesicular GABA transporter knockout mice. Front Cell Neurosci. 2014;7:1–11.

15. White JJ, Arancillo M, Stay TL, George-Jones NA, Levy SL, Heck DH, et al. Cerebellar zonal patterning relies on purkinje cell neurotransmission. J Neurosci. 2014;34:8231–45.

16. Obata K, Hirono M, Kume N, Kawaguchi Y, Itohara S, Yanagawa Y. GABA and synaptic inhibition of mouse cerebellum lacking glutamate decarboxylase 67. Biochem Biophys Res Commun. 2008;370:429–33.

17. Fujihara K, Miwa H, Kakizaki T, Kaneko R, Mikuni M, Tanahira C, et al. Glutamate Decarboxylase 67 Deficiency in a Subset of GABAergic Neurons Induces Schizophrenia-Related Phenotypes. Neuropsychopharmacology. 2015;40:2475–86.

487 18. Kuki T, Fujihara K, Miwa H, Tamamaki N, Yanagawa Y, Mushiake H.
488 Contribution of parvalbumin and somatostatin-expressing gabaergic neurons to slow
489 oscillations and the balance in beta-gamma oscillations across cortical layers. Front
490 Neural Circuits. 2015;9:1–12.
491 19. Tamamaki N, Yanagawa Y, Tomioka R, Miyazaki J-I, Obata K, Kaneko T. Green
492 fluorescent protein expression and colocalization with calretinin, parvalbumin, and
493 somatostatin in the GAD67-GFP knock-in mouse. J Comp Neurol. 2003;467:60–79.
494 20. Tanahira C, Higo S, Watanabe K, Tomioka R, Ebihara S, Kaneko T, et al.
495 Parvalbumin neurons in the forebrain as revealed by parvalbumin-Cre transgenic mice.
496 Neurosci Res. 2009;63:213–23.
497 21. Obata K, Hirono M, Kume N, Kawaguchi Y, Itohara S, Yanagawa Y. GABA and
498 synaptic inhibition of mouse cerebellum lacking glutamate decarboxylase 67. Biochem
499 Biophys Res Commun. 2008;370:429–33.
500 22. Fukaya M, Tsujita M, Yamazaki M, Kushiya E, Abe M, Akashi K, et al. Abundant
501 distribution of TARP gamma-8 in synaptic and extrasynaptic surface of hippocampal

neurons and its major role in AMPA receptor expression on spines and dendrites. Eur J Neurosci. 2006;24:2177–90.

23. Schwaller B, Meyer M, Schiffmann S. “New” functions for “old” proteins: The role of the calcium-binding proteins calbindin D-28k, calretinin and parvalbumin, in cerebellar physiology. Studies with knockout mice. The Cerebellum. 2002;1:241–58.

24. Bastianelli E. Distribution of calcium-binding proteins in the cerebellum. The Cerebellum. 2003;2:242–62.

25. Hirono M, Watanabe S, Karube F, Fujiyama F, Kawahara S, Nagao S, et al. Perineuronal nets in the deep cerebellar nuclei regulate GABAergic transmission and delay eyeblink conditioning. J Neurosci. 2018;38:6130–44.

26. McNamara NM, Muniz ZM, Wilkin GP, Dolly JO. Prominent location of a K+ channel containing the alpha subunit Kv 1.2 in the basket cell nerve terminals of rat cerebellum. Neuroscience. 1993;57:1039–45.

27. Laube G, Röper J, Pitt JC, Sewing S, Kistner U, Garner CC, et al. Ultrastructural localization of Shaker-related potassium channel subunits and synapse-associated

517 protein 90 to septate-like junctions in rat cerebellar Pinceaux. Brain Res Mol Brain Res.
518 1996;42:51–61.
519 28. Buttermore ED, Piochon C, Wallace ML, Philpot BD, Hansel C, Bhat MA. Pinceau
520 organization in the cerebellum requires distinct functions of neurofascin in purkinje and
521 basket neurons during postnatal development. J Neurosci. 2012;32:4724–42.
522 29. Le Magueresse C, Monyer H. GABAergic Interneurons Shape the Functional
523 Maturation of the Cortex. Neuron. 2013;77:388–405.
524 30. Murata Y, Colonnese MT. GABAergic interneurons excite neonatal hippocampus in
525 vivo. Sci Adv. 2020;6:1–11.
526 31. Ben-Ari Y, Khalilov I, Represa A, Gozlan H. Interneurons set the tune of
527 developing networks. Trends Neurosci. 2004;27:422–7.
528 32. Ben-Ari Y. Excitatory actions of GABA during development: The nature of the
529 nurture. Nat Rev Neurosci. 2002;3:728–39.
530 33. Condie BG, Bain G, Gottlieb DI, Capecchi MR. Cleft palate in mice with a targeted
531 mutation in the γ-aminobutyric acid-producing enzyme glutamic acid decarboxylase 67.
532 Proc Natl Acad Sci U S A. 1997;94:11451–5.

533 34. Tian N, Petersen C, Kash S, Baekkeskov S, Copenhagen D, Nicoll R. The role of
534 the synthetic enzyme GAD65 in the control of neuronal γ-aminobutyric acid release.
535 Proc Natl Acad Sci U S A. 1999;96:12911–6.
536 35. Kiser PJ, Cooper NGF, Mower GD. Expression of two forms of glutamic acid
537 decarboxylase (GAD67 and GAD65) during postnatal development of rat
538 somatosensory barrel cortex. J Comp Neurol. 1998;402:62–74.
539 36. Ango F, Di Cristo G, Higashiyama H, Bennett V, Wu P, Huang ZJ. Ankyrin-based
540 subcellular gradient of neurofascin, an immunoglobulin family protein, directs
541 GABAergic innervation at Purkinje axon initial segment. Cell. 2004;119:257–72.
542 37. Brown AM, Arancillo M, Lin T, Catt DR, Zhou J, Lackey EP, et al. Molecular layer
543 interneurons shape the spike activity of cerebellar Purkinje cells. Sci Rep. 2019;9:1–19.
544 38. Chung YH, Shin CM, Kim MJ, Lee BK, Cha CI. Immunohistochemical study on the
545 distribution of six members of the Kv1 channel subunits in the rat cerebellum. Brain
546 Res. 2001;895:173–7.

547 39. Rhodes KJ, Strassle BW, Monaghan MM, Bekele-Arcuri Z, Matos MF, Trimmer JS.
548 Association and colocalization of the Kvβ1 and Kvβ2 β-subunits with Kv1 α-subunits in
549 mammalian brain K^+ channel complexes. J Neurosci. 1997;17:8246–58.
550 40. Yang J-W, Vacher H, Park K-S, Clark E, Trimmer JS. Trafficking-dependent
551 phosphorylation of Kv1.2 regulates voltage-gated potassium channel cell surface
552 expression. Proc Natl Acad Sci U S A. 2007;104:20055–60.
553 41. Bin Tean Teh, Silburn P, Lindblad K, Betz R, Boyle R, Schalling M, et al. Familial
554 periodic cerebellar ataxia without myokymia maps to a 19-cM region on 19p13. Am J
555 Hum Genet. 1995;56:1443–9.
556 42. D'Adamo MC, Gallenmüller C, Servettini I, Hartl E, Tucker SJ, Arning L, et al.
557 Novel phenotype associated with a mutation in the KCNA1(Kv1.1) gene. Front Physiol.
558 2015;6:1–10.
559 43. Browne DL, Gancher ST, Nutt JG, Brunt ER, Smith EA, Kramer P, et al. Episodic
560 ataxia/myokymia syndrome is associated with point mutations in the human
561 potassium channel gene, KCNA1. Nat Genet. 1994;8:136–40.

562 44. Manto M, Honnorat J, Hampe CS, Guerra-Narbona R, López-Ramos JC, Delgado-
563 García JM, et al. Disease-specific monoclonal antibodies targeting glutamate
564 decarboxylase impair GABAergic neurotransmission and affect motor learning and
565 behavioral functions. Front Behav Neurosci. 2015;9:1–14.
566
567

Figure legends

Fig. 1. Normal cerebellar morphology in *PV-Cre:GAD67*$^{flox/flox}$ mice. (**a**) Quantification of body weight. (**b**) Expression of Cre recombinase (Cre) in parvalbumin (PV)-positive cells leads to Cre-mediated ablation of *GAD67* and the loss of glutamate decarboxylase 67 (GAD67) immunoreactivity in the cerebellum of *PV-Cre*; *GAD67*$^{flox/flox}$ mice. ML, molecular layer; PL, Purkinje cell layer. Scale bar, 50 μm. (**c**) Quantification of the percentage of Cre-positive cells that express PV (left bar) and percentage of PV-positive cells that express Cre (right bar). (**d**) Quantification of the number of PV-positive cells in the molecular layer (left) and in the PL (right). (**e**) Sagittal sections of the cerebellum from control (*GAD67*$^{flox/flox}$) and mutant (*PV-Cre*; *GAD67*$^{flox/flox}$) mice. Purkinje cells are labeled with calbindin (green), and the granular layer is particularly highlighted by DAPI staining (blue). Scale bar, 500 μm. (**f**) Quantification of molecular layer thickness.

Fig. 2. GAD expression in the cerebellar cortex and deep cerebellar nuclei (DCN). (**a**) Immunohistochemistry for GAD67 (cyan), GAD65 (yellow), and calbindin (CB; magenta) in the cerebellar cortices of control (*GAD67*$^{flox/flox}$) and mutant (*PV-Cre*; *GAD67*$^{flox/flox}$) mice. Scale bar, 50 μm. ML, molecular layer; PL, Purkinje cell layer. (**b**) Quantification of immunoreactive signals for GAD67 (left) and GAD65 (right) in the molecular layer of the cerebellum. (**c**) Quantification of immunoreactive signals for GAD67 (left), GAD65 (middle), and calbindin (right) in the Purkinje cell layer of the cerebellum. (**d**) Immunohistochemistry for GAD67 (cyan), GAD65 (yellow), and calbindin (magenta) in the DCN of control (*GAD67*$^{flox/flox}$) and mutant (*PV-Cre*;

591 *GAD67*$^{flox/flox}$) mice. (**e**) Quantification of immunoreactive signals for GAD67 (left),
592 GAD65 (middle), and calbindin (right) in the DCN. Scale bar, 200 μm. ****$P < 0.0001$.
593
594 **Fig. 3.** *GAD67* deletion from parvalbumin neurons does not affect parallel fiber
595 synapses or climbing fiber synapse density. (**a**) Immunohistochemistry for VGluT1
596 (cyan), VGluT2 (yellow), and calbindin (CB; magenta) in the cerebellar cortices of
597 control (*GAD67*$^{flox/flox}$) and mutant (*PV-Cre*; *GAD67*$^{flox/flox}$) mice. Scale bar, 20 μm.
598 ML, molecular layer; PL, Purkinje cell layer. (**b**) Quantification of parallel fiber synapse
599 and climbing fiber synapse density (bottom) via VGluT1 staining intensity (top) and
600 counts of VGluT2-positve puncta per 100 μm^2 (bottom).
601
602 **Fig. 4.** *GAD67* deletion from parvalbumin neurons does not affect VGAT-positive
603 inhibitory synapses in the cerebellum. (**a**) Immunohistochemistry for VGAT (green) and
604 calbindin (CB; magenta) in the cerebellar cortices of control (*GAD67*$^{flox/flox}$) and mutant
605 (*PV-Cre*; *GAD67*$^{flox/flox}$) mice. Scale bar, 20 μm. ML, molecular layer; PL, Purkinje cell
606 layer. (**b**) Quantification of VGAT-positive puncta per 100 μm^2 in the molecular layer
607 of the cerebellum.
608
609 **Fig. 5.** Aberrant subcellular Kv1.1 localization and basket cell projections in *PV-Cre*;
610 *GAD67*$^{flox/flox}$ mice. (**a**) Immunohistochemistry for Kv1.1 (green) and calbindin (CB;
611 magenta) in the cerebellar cortices of control (*GAD67*$^{flox/flox}$) and mutant (*PV-Cre*;
612 *GAD67*$^{flox/flox}$) mice. The images represent maximum-intensity projections of a confocal
613 image stack. Scale bar, 20 μm. ML, molecular layer; PL, Purkinje cell layer. (**b**) Higher

magnification images of the corresponding white boxes in panel **a**. (**c**) Plot profiles of the fluorescence intensities for Kv1.1 along the yellow lines shown in **b** up to 50 μm from the axon hillock. Shading indicates SEMs. (**d**) Summation of the fluorescence intensities for Kv1.1 in plot profiles at a distance from 0 to 10 μm from the axon hillock. (**e**) Immunohistochemistry for neurofilaments (Nfl) (green) and calbindin (magenta) in the cerebellar cortices of control (*GAD67*$^{flox/flox}$) and mutant (*PV-Cre*; *GAD67*$^{flox/flox}$) mice. The images represent maximum-intensity projections of a confocal image stack. Scale bar, 20 μm. (**f**) Higher magnification images of the corresponding white boxes in panel **e**. (**g**) Plot profiles of the fluorescence intensities of neurofilaments along the yellow lines in panel **f** at a distance of 50 μm from the axon hillock. Shading indicates SEMs. (**h**) Summation of the fluorescence intensities for Nfl in plot profiles at a distance from 0 to 50 μm from the axon hillock in **g**. **P* < 0.05, ***P* < 0.01.

Fig. 6. Aberrant basket cell projections to Purkinje cells in *GAD65* KO mice. (**a**) Immunohistochemistry for Kv1.1 (green) and calbindin (CB; magenta) in the cerebellar cortices of wild-type (*GAD67*$^{+/+}$) and *GAD65* KO (*GAD65*$^{-/-}$) mice. The images represent maximum-intensity projections of a confocal image stack. Scale bar, 20 μm. ML, molecular layer; PL, Purkinje cell layer. (**b**) Higher magnification images of the corresponding white boxes in panel **a**. (**c**) Plot profiles of the fluorescence intensities for Kv1.1 along the yellow lines in **b** at a distance of up to 50 μm from the axon. Shading indicates SEMs. (**d**) Summation of the fluorescence intensities for Kv1.1 in plot profiles at a distance from 0 to 10 μm from the axon hillock. (**e**) Immunohistochemistry for neurofilaments (Nfl; green) and calbindin (magenta) in the cerebellar cortices of wild-

type (*GAD67*$^{+/+}$) and *GAD65* KO (*GAD67*$^{-/-}$) mice. The images represent maximum-intensity projections of a confocal image stack. Scale bar, 20 μm. (**f**) Higher magnification images of the corresponding white boxes in panel **e**. (**g**) Plot profiles of the fluorescence intensities of neurofilaments along the yellow lines in panel **f** at a distance of 50 μm from the axon hillock. Shading indicates SEMs. (**h**) Summation of the fluorescence intensities for Nfl in plot profiles at a distance from 0 to 50 μm from the axon hillock. *$P < 0.05$.

Fig. 7. Motor coordination deficits in *PV-Cre:GAD67*$^{flox/flox}$ mice. (**a**) Accelerating rotarod test. Mice were trained for eight trials, four trials per day for 2 consecutive days. Rotarod performance of *PV-Cre:GAD67*$^{flox/flox}$ and control *GAD67*$^{flox/flox}$ at constant speeds of 5 rpm (**b**) and 10 rpm (**c**). (**d**) Sample footprints from *GAD67*$^{flox/flox}$ (left) and *PV-Cre*; *GAD67*$^{flox/flox}$ mice (right). (**e**) Quantification of footprints in terms of stride, sway, and stance. (**f**) Average latency to fall from the wire mesh in the wire hang test.

Supplementary materials

Additional file 1. Body weight changes and survival curves of *PV-Cre*; *VGAT*$^{flox/flox}$ mice. (**a**) Average body weights of *VGAT*$^{flox/flox}$ and *PV-Cre*; *VGAT*$^{flox/flox}$ mice. Significant differences were observed between two genotypes [$F(1,6) = 0.0106$, $P = 0.0106$; two-way repeated measures ANOVA]. Results shown are the means ± SEMs ($n = 4$ mice per genotype). (**b**) Survival curves of *VGAT*$^{flox/flox}$ ($n = 4$) and *PV-Cre*; *VGAT*$^{flox/flox}$ ($n = 4$) mice ($P = 0.0833$, log-rank test). (**c**) Comparison of *VGAT*$^{flox/flox}$ (left) and *PV-Cre*; *VGAT*$^{flox/flox}$ (right) mice at postnatal day 12. *PV-Cre*; *VGAT*$^{flox/flox}$ mice exhibited generalized convulsive seizures.

Additional file 2. Confirmation of antibody specificity using knockout mice. (**a**) GAD67 immunohistochemistry of sagittal sections of wild-type and *GAD67*$^{GFP/GFP}$ mice at P0. GE, ganglionic eminence. Scale bar, 500 μm. (**b**) GAD65 immunohistochemistry in the cerebellar cortices of wild-type and *GAD65*$^{-/-}$ mice at 8 weeks old. Scale bar, 50 μm. ML, molecular layer; PL, Purkinje cell layer.

Additional file 3. Normal perineuronal nets and no ectopic expression of tyrosine hydroxylase in *PV-Cre*; *GAD67*$^{flox/flox}$ mice. (**a**) Perineuronal nets in the deep cerebellar nuclei are unaltered in *PV-Cre*; *GAD67*$^{flox/flox}$ mice. The large neurons (identified by NeuroTrace; magenta) are enwrapped by perineuronal nets identified by an antibody against *Wisteria floribunda* agglutinin (WFA; green). Scale bar, 200 μm. (**b)** Immunohistochemistry of coronal cerebellar sections for zebrin II and tyrosine hydroxylase (TH). Purkinje cells in *PV-Cre*; *GAD67*$^{flox/flox}$ mice exhibit no ectopic

676 expression of TH. Cellular expression pattern of zebrin II (green) is unaltered in *PV-*
677 *Cre*; *GAD67*$^{flox/flox}$ mice. Scale bar, 500 μm.
678
679 **Additional file 4.** Normal VGluT1-positive parallel fiber synapses, VGluT2-positive
680 climbing fiber synapses, and VGAT-positive inhibitory synapses in *GAD65* KO mice.
681 (**a**) Immunohistochemistry for GAD67 (cyan), GAD65 (yellow), and calbindin (CB;
682 magenta) in the cerebellar cortices of wild-type (*GAD65*$^{+/+}$) and *GAD65* KO (*GAD65*$^{-/-}$)
683 mice. Scale bar, 50 μm. ML, molecular layer; PL, Purkinje cell layer. (**b**) Quantification
684 of immunoreactive signals for GAD67 (left) and GAD65 (right) in the molecular layer
685 of the cerebellum. (**c**) Quantification of immunoreactive signals for GAD67 (left),
686 GAD65 (middle), and calbindin (right) in the PL of the cerebellum. (**d**)
687 Immunohistochemistry for VGluT1 (cyan), VGluT2 (yellow), and calbindin (magenta)
688 in the cerebellar cortices of wild-type (*GAD65*$^{+/+}$) and *GAD65* KO (*GAD65*$^{-/-}$) mice.
689 Scale bar, 20 μm. (**e**) Quantification of parallel fiber synapses and climbing fiber
690 synapse density byVGluT1-positive staining intensity (left) and counts of VGluT2-
691 positve puncta per 100 μm^2 (right). (**f**) Immunohistochemistry for VGAT (green) and
692 parvalbumin (PV; magenta) in the cerebellar cortices of wild-type (*GAD65*$^{+/+}$) and
693 *GAD65* KO (*GAD65*$^{-/-}$) mice. Scale bar, 20 μm. (**g**) Quantification of VGAT-positive
694 puncta per 100 μm^2 in the molecular layer of the cerebellum (left), and the numbers of
695 PV-positive cells in the molecular layer (middle) and in the Purkinje cell layer (right).
696 *$P < 0.05$, **$P < 0.01$.

Figures

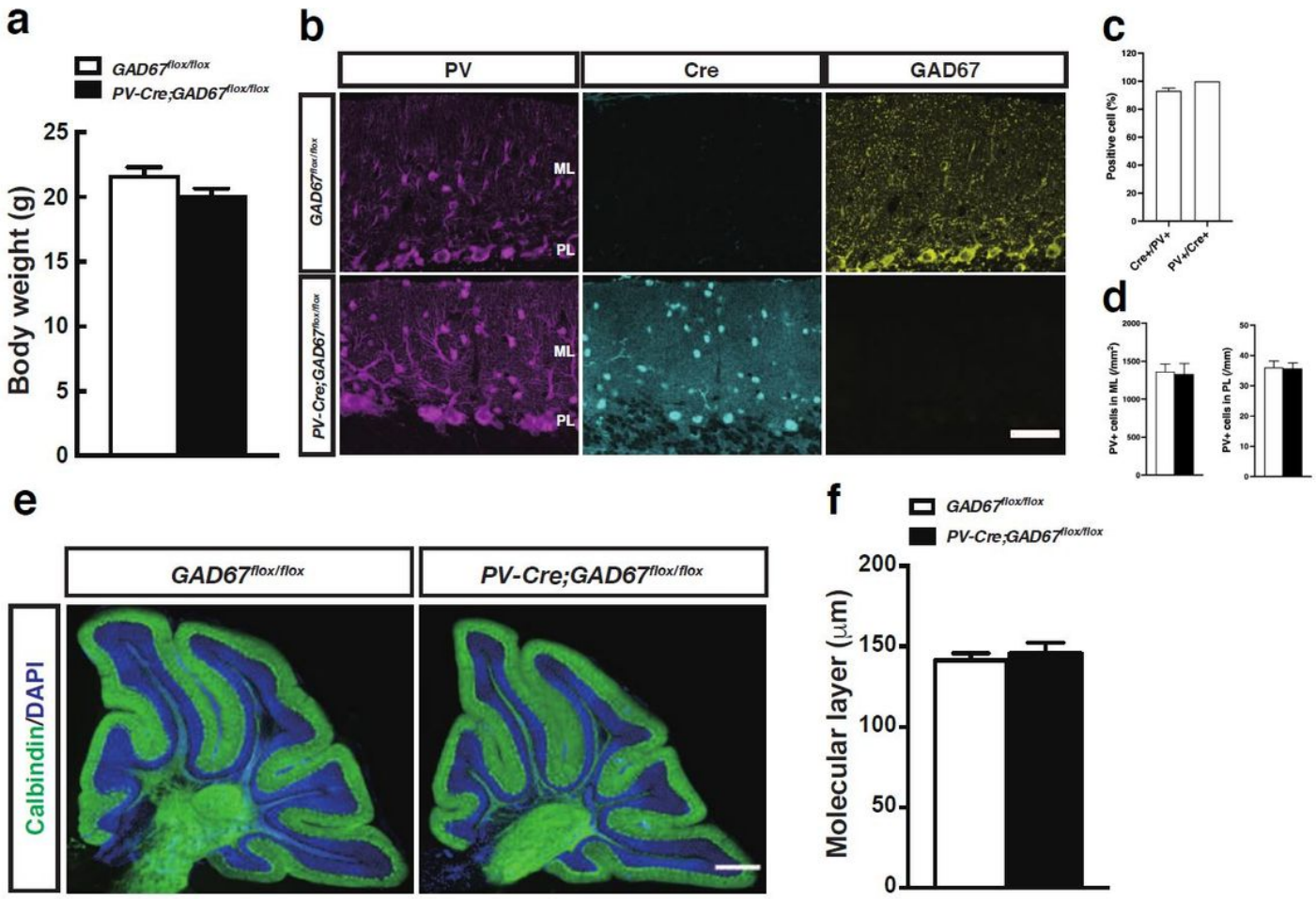

Figure 1

Normal cerebellar morphology in PV-Cre:GAD67flox/flox mice. (a) Quantification of body weight. (b) Expression of Cre recombinase (Cre) in parvalbumin (PV)-positive cells leads to Cre-mediated ablation of GAD67 and the loss of glutamate decarboxylase 67 (GAD67) immunoreactivity in the cerebellum of PV-Cre; GAD67flox/flox mice. ML, molecular layer; PL, Purkinje cell layer. Scale bar, 50 μm. (c) Quantification of the percentage of Cre-positive cells that express PV (left bar) and percentage of PV-positive cells that express Cre (right bar). (d) Quantification of the number of PV-positive cells in the molecular layer (left) and in the PL (right). (e) Sagittal sections of the cerebellum from control (GAD67flox/flox) and mutant (PV-Cre; GAD67flox/flox) mice. Purkinje cells are labeled with calbindin (green), and the granular layer is particularly highlighted by DAPI staining (blue). Scale bar, 500 μm. (f) Quantification of molecular layer thickness.

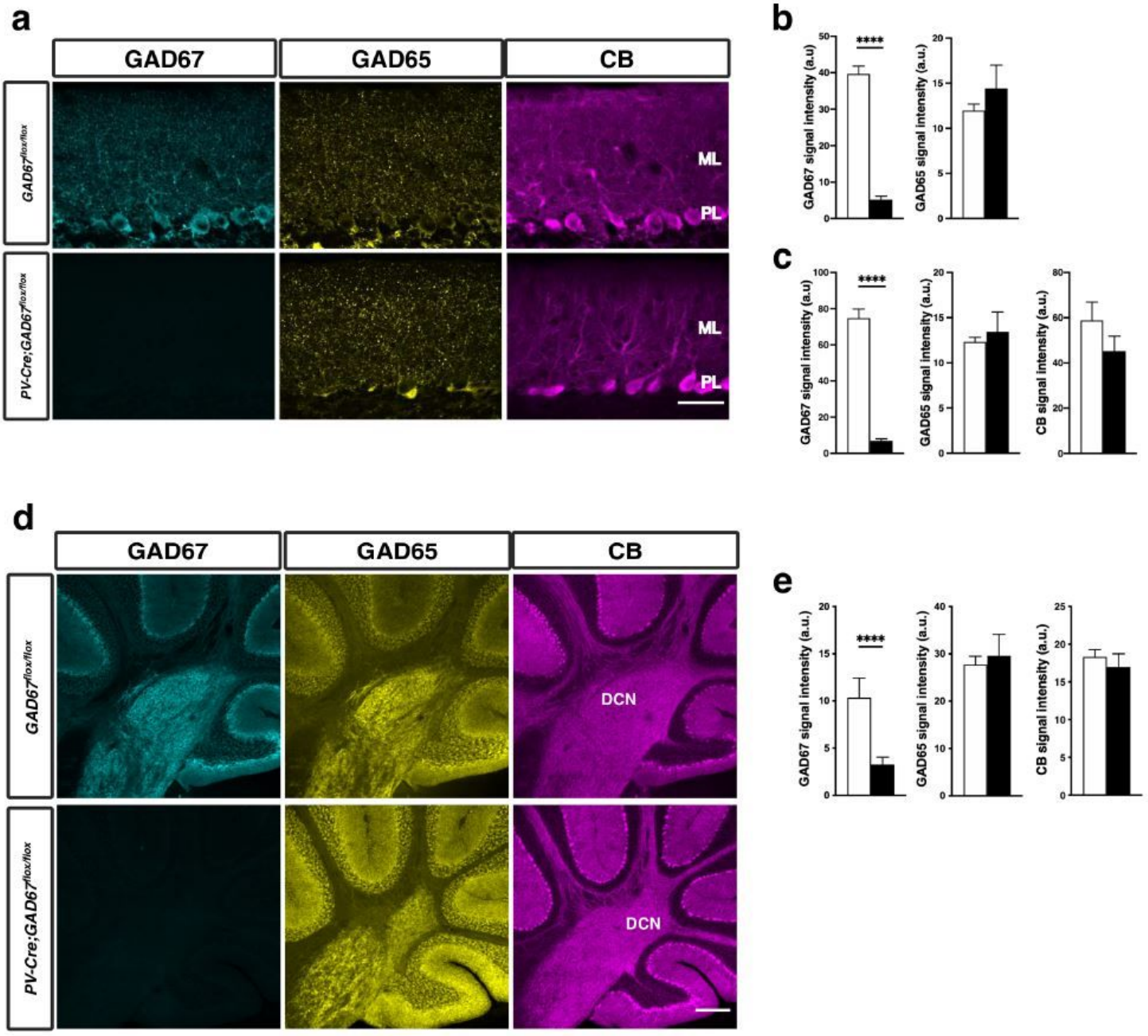

Figure 2

GAD expression in the cerebellar cortex and deep cerebellar nuclei (DCN). (a) Immunohistochemistry for GAD67 (cyan), GAD65 (yellow), and calbindin (CB; magenta) in the cerebellar cortices of control (GAD67flox/flox) and mutant (PV-Cre; GAD67flox/flox) mice. Scale bar, 50 μm. ML, molecular layer; PL, Purkinje cell layer. (b) Quantification of immunoreactive signals for GAD67 (left) and GAD65 (right) in the molecular layer of the cerebellum. (c) Quantification of immunoreactive signals for GAD67 (left), GAD65 (middle), and calbindin (right) in the Purkinje cell layer of the cerebellum. (d) Immunohistochemistry for GAD67 (cyan), GAD65 (yellow), and calbindin (magenta) in the DCN of control (GAD67flox/flox) and mutant (PV-Cre; GAD67flox/flox) mice. (e) Quantification of immunoreactive signals for GAD67 (left), GAD65 (middle), and calbindin (right) in the DCN. Scale bar, 200 μm. ****P < 0.0001.

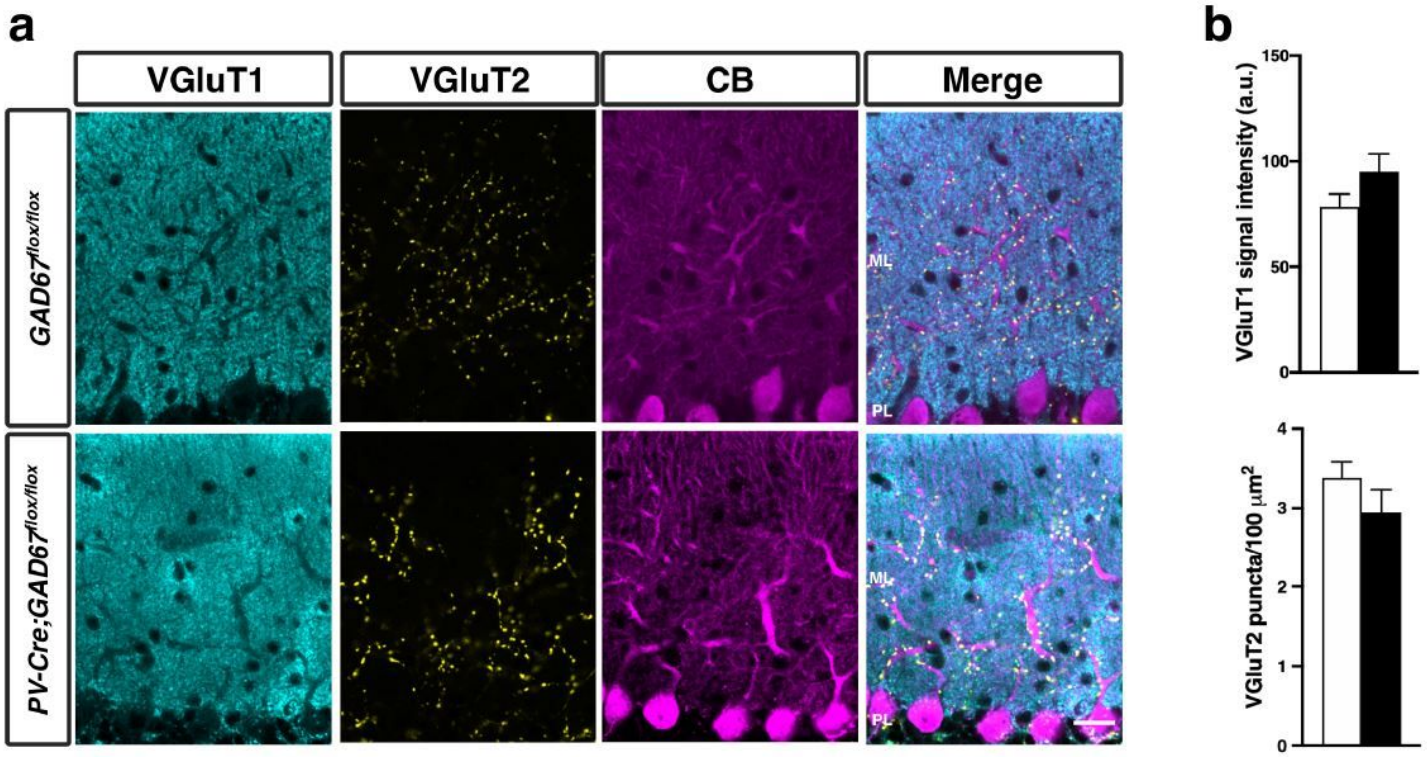

Figure 3

GAD67 deletion from parvalbumin neurons does not affect parallel fiber synapses or climbing fiber synapse density. (a) Immunohistochemistry for VGluT1 (cyan), VGluT2 (yellow), and calbindin (CB; magenta) in the cerebellar cortices of control (GAD67flox/flox) and mutant (PV-Cre; GAD67flox/flox) mice. Scale bar, 20 μm. ML, molecular layer; PL, Purkinje cell layer. (b) Quantification of parallel fiber synapse and climbing fiber synapse density (bottom) via VGluT1 staining intensity (top) and counts of VGluT2-positve puncta per 100 μm2 (bottom).

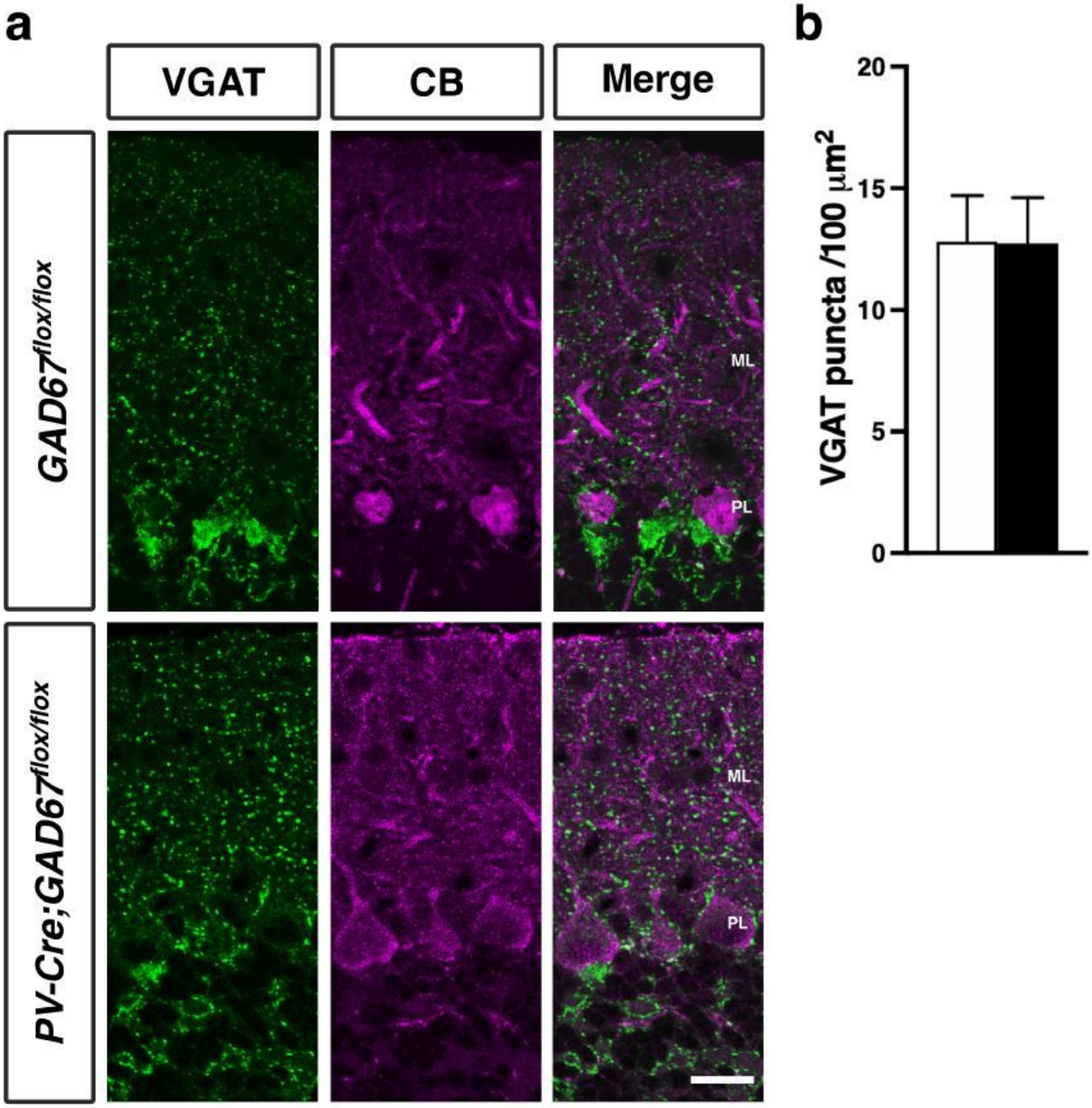

Figure 4

GAD67 deletion from parvalbumin neurons does not affect VGAT-positive inhibitory synapses in the cerebellum. (a) Immunohistochemistry for VGAT (green) and calbindin (CB; magenta) in the cerebellar cortices of control (GAD67flox/flox) and mutant (PV-Cre; GAD67flox/flox) mice. Scale bar, 20 μm. ML, molecular layer; PL, Purkinje cell layer. (b) Quantification of VGAT-positive puncta per 100 μm2 in the molecular layer of the cerebellum.

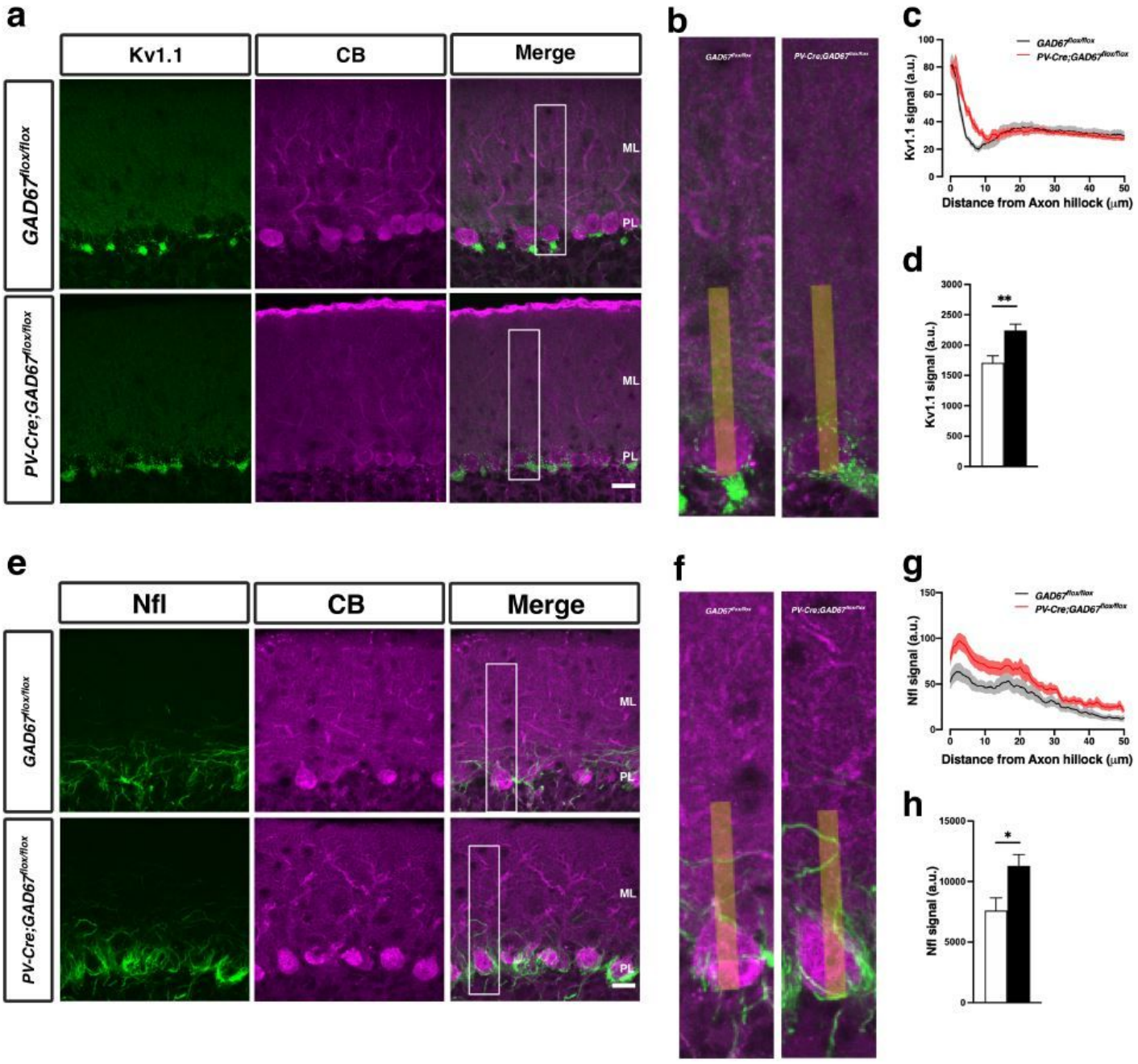

Figure 5

Aberrant subcellular Kv1.1 localization and basket cell projections in PV-Cre; GAD67flox/flox mice. (a) Immunohistochemistry for Kv1.1 (green) and calbindin (CB; magenta) in the cerebellar cortices of control (GAD67flox/flox) and mutant (PV-Cre; GAD67flox/flox) mice. The images represent maximum-intensity projections of a confocal image stack. Scale bar, 20 μm. ML, molecular layer; PL, Purkinje cell layer. (b) Higher magnification images of the corresponding white boxes in panel a. (c) Plot profiles of the fluorescence intensities for Kv1.1 along the yellow lines shown in b up to 50 μm from the axon hillock. Shading indicates SEMs. (d) Summation of the fluorescence intensities for Kv1.1 in plot profiles at a distance from 0 to 10 μm from the axon hillock. (e) Immunohistochemistry for neurofilaments (Nfl) (green) and calbindin (magenta) in the cerebellar cortices of control (GAD67flox/flox) and mutant (PV-

Cre; GAD67flox/flox) mice. The images represent maximum-intensity projections of a confocal image stack. Scale bar, 20 μm. (f) Higher magnification images of the corresponding white boxes in panel e. (g) Plot profiles of the fluorescence intensities of neurofilaments along the yellow lines in panel f at a distance of 50 μm from the axon hillock. Shading indicates SEMs. (h) Summation of the fluorescence intensities for Nfl in plot profiles at a distance from 0 to 50 μm from the axon hillock in g. *P < 0.05, **P < 0.01.

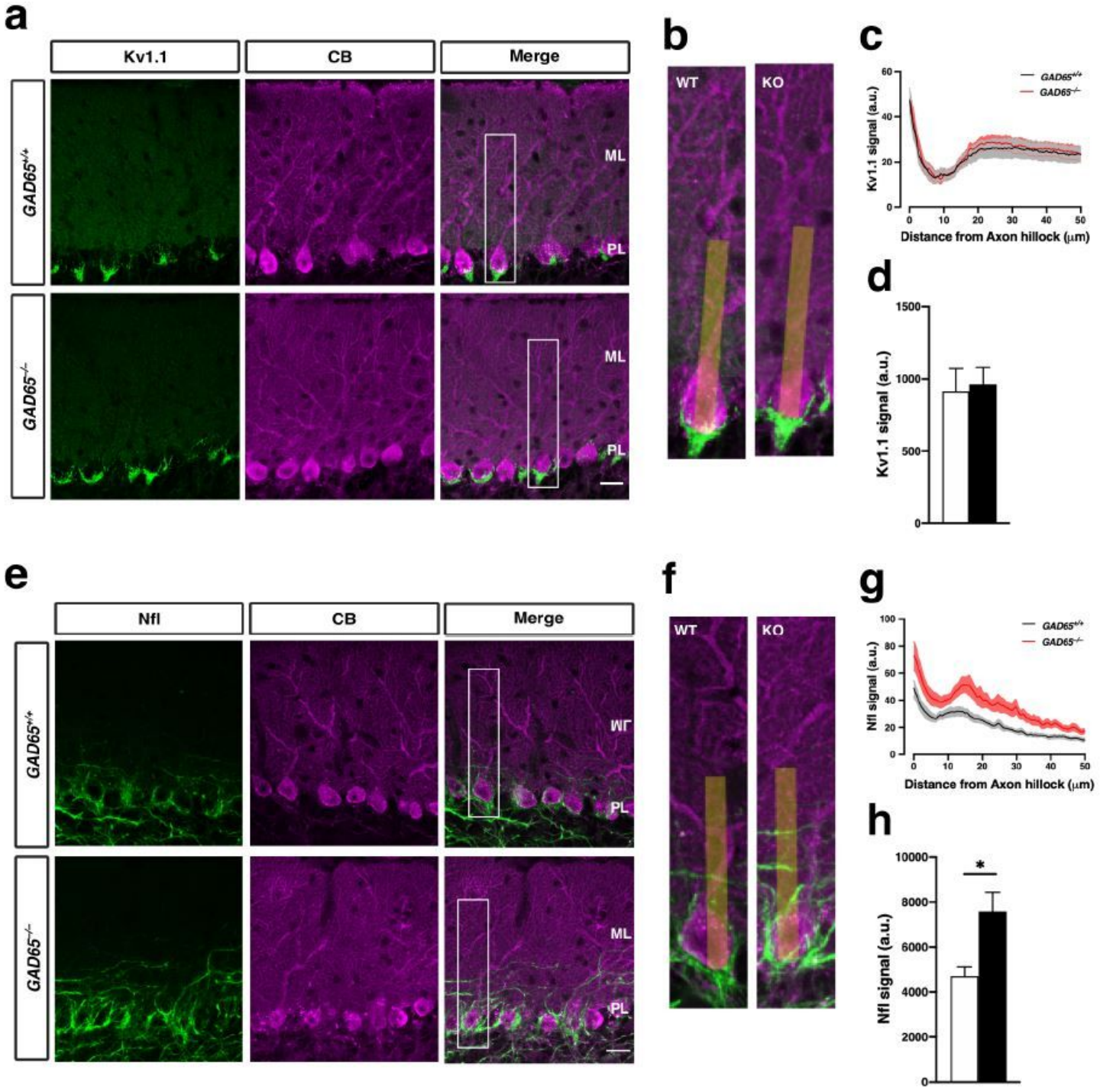

Figure 6

Aberrant basket cell projections to Purkinje cells in GAD65 KO mice. (a) Immunohistochemistry for Kv1.1 (green) and calbindin (CB; magenta) in the cerebellar cortices of wild-type (GAD67+/+) and GAD65 KO (GAD65−/−) mice. The images represent maximum-intensity projections of a confocal image stack. Scale bar, 20 μm. ML, molecular layer; PL, Purkinje cell layer. (b) Higher magnification images of the corresponding white boxes in panel a. (c) Plot profiles of the fluorescence intensities for Kv1.1 along the yellow lines in b at a distance of up to 50 μm from the axon. Shading indicates SEMs. (d) Summation of the fluorescence intensities for Kv1.1 in plot profiles at a distance from 0 to 10 μm from the axon hillock. (e) Immunohistochemistry for neurofilaments (Nfl; green) and calbindin (magenta) in the cerebellar cortices of wild32 type (GAD67+/+) and GAD65 KO (GAD67−/−) mice. The images represent maximum intensity projections of a confocal image stack. Scale bar, 20 μm. (f) Higher magnification images of the corresponding white boxes in panel e. (g) Plot profiles of the fluorescence intensities of neurofilaments along the yellow lines in panel f at a distance of 50 μm from the axon hillock. Shading indicates SEMs. (h) Summation of the fluorescence intensities for Nfl in plot profiles at a distance from 0 to 50 μm from the axon hillock. *P < 0.05.

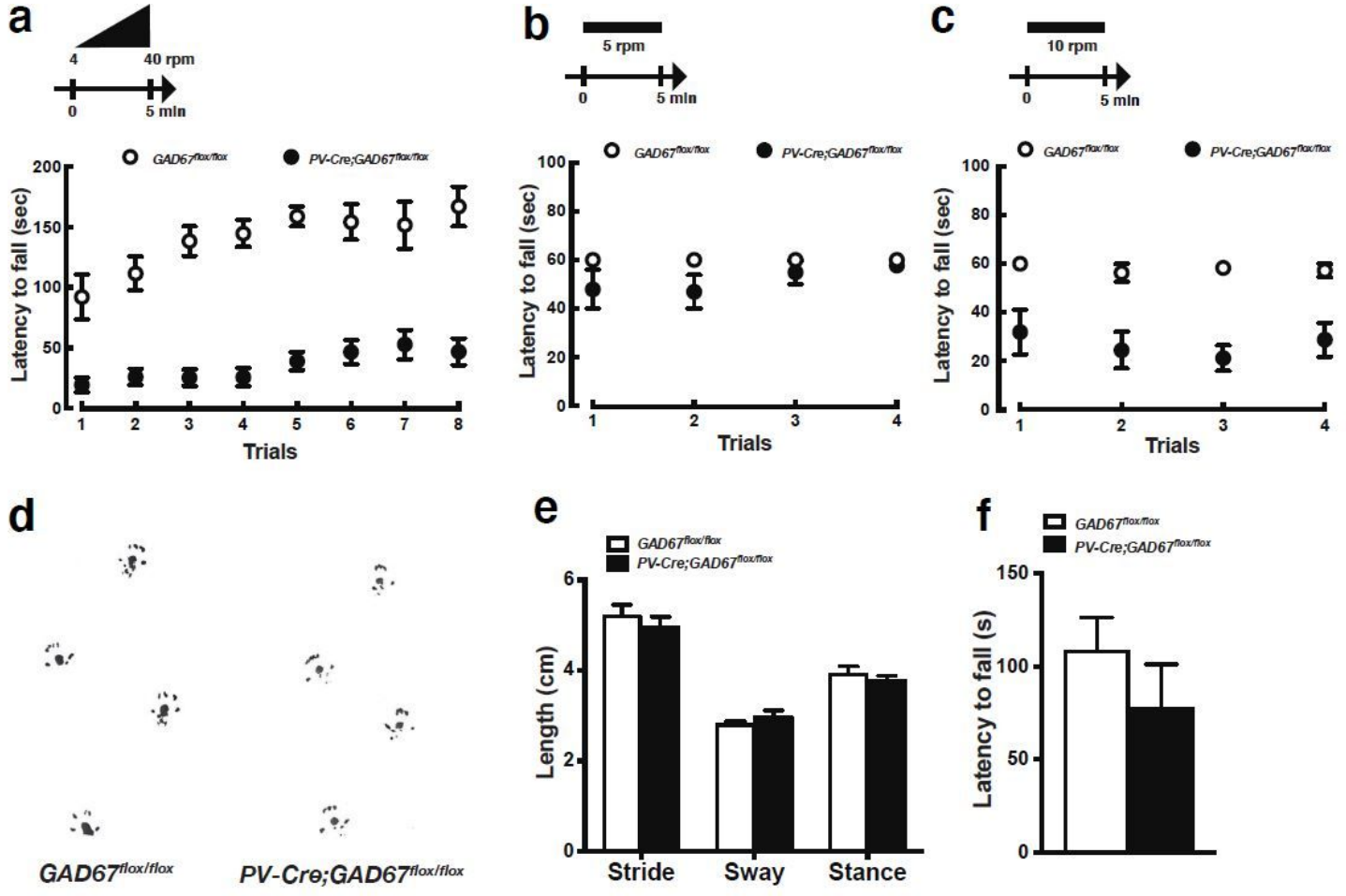

Figure 7

Motor coordination deficits in PV-Cre:GAD67flox/flox mice. (a) Accelerating rotarod test. Mice were trained for eight trials, four trials per day for 2 consecutive days. Rotarod performance of PV-Cre:GAD67flox/flox and control GAD67flox/flox at constant speeds of 5 rpm (b) and 10 rpm (c). (d)

Sample footprints from GAD67flox/flox (left) and PV-Cre; GAD67flox/flox mice (right). (e) Quantification of footprints in terms of stride, sway, and stance. (f) Average latency to fall from the wire mesh in the wire hang test.

Supplementary Files

This is a list of supplementary files associated with this preprint. Click to download.

- Additionalfile1.JPG
- Additionalfile2.JPG
- Additionalfile3.JPG
- Additionalfile4.JPG